EUV spectra of Rb-like to Cu-like gadolinium ions in an electron-beam ion trap

D. Kilbane* and G. O'Sullivan
School of Physics, University College Dublin, Belfield, Dublin 4, Ireland

J. D. Gillaspy, Yu. Ralchenko, and J. Reader
National Institute of Standards and Technology, Gaithersburg, Maryland 20899, USA

(Received 16 August 2012; published 8 October 2012)

Measurements of extreme ultraviolet radiation from highly charged gadolinium ions were made at the National Institute of Standards and Technology. The ions were produced and confined in an electron-beam ion trap (EBIT), and the spectra were recorded with a flat-field grazing-incidence spectrometer in the wavelength range 3–17 nm. Ionization stages from Rb-like to Cu-like gadolinium were selected by tuning the electron-beam energies between 0.97 and 1.7 keV. Strong intrashell $n = 4$–$n = 4$ transitions were identified by performing detailed collisional-radiative modeling of the EBIT plasma. A total of 73 spectral features were recorded, including 59 new identifications.

DOI: 10.1103/PhysRevA.86.042503 PACS number(s): 32.30.Jc, 32.70.−n, 31.15.A−

I. INTRODUCTION

Characterization of extreme ultraviolet (EUV) radiation emitted from gadolinium and terbium ions is of great importance to the semiconductor industry, as these are the proposed next-generation lithographic sources at wavelengths shorter than 13.5 nm [1]. The atomic processes in Gd and Tb have been successfully modeled, with $4d$-$4f$ and $4p$-$4d$ transitions identified as giving rise to large emission at 6.75 nm [1–5]. In this work we move to higher ion stages and classify the strong $n = 4$–$n = 4$ transitions that occur in Rb-like to Cu-like gadolinium ions.

EUV radiation from highly charged gadolinium ions has been observed previously in laser-produced plasmas and tokamak devices: Cu-like [6–11], Zn-like [10–14], and Ga-like [10,11,14], and more recently, in the Large Helical Device (LHD) at the National Institute for Fusion Science (NIFS) [15]. Theoretical works include wavelength and energy-level multiconfiguration Dirac-Fock calculations of the Cu isoelectronic sequence performed by Seely *et al.* with the Grant code [9,16], Sugar *et al.* [17] using the Desclaux code [18], and Kim *et al.* [19], who included quantum-electrodynamic (QED) corrections in the Desclaux code simulations. Similar calculations for the Zn isoelectronic sequence were carried out by Brown *et al.* using the Hebrew University Lawrence Livermore Atomic Code (HULLAC) [20,21]. The results of *ab initio* atomic structure calculations of Ga-like gadolinium using the parametric potential code RELAC, the relativistic version of MAPPAC [22,23], were presented in [11].

In this paper we report EUV measurements of Gd^{27+}-Gd^{35+} spectral lines in an electron-beam ion trap (EBIT) and their identifications. To our knowledge this study of Rb-like to Ge-like gadolinium spectra has not been done before. It extends other work carried out at the National Institute of Standards and Technology (NIST) on $n = 4$–$n = 4$ EUV transitions in tungsten, hafnium, tantalum, and gold [24,25], and it can be used for diagnostics of hot plasmas in fusion devices and for studies of trends in atomic structure. Excellent agreement between observed and calculated spectra led to the identification of 73 lines and further validated the use of collisional-radiative (CR) codes such as NOMAD [26] in modeling of EBIT plasmas.

The outline of this paper is as follows. In Sec. II a brief overview of the EBIT experiment is given. Collisional-radiative modeling of the EBIT spectra is discussed in Sec. III, and the resulting line identifications are presented in Sec. IV. Finally, in Sec. V we conclude with a summary.

II. EXPERIMENT

The measurements were performed at the EBIT facility at NIST. A detailed description of the NIST EBIT can be found in [27] and only a brief outline is given here. The EBIT consists of a tightly focused, tunable energy electron beam that creates, traps, and excites highly charged ions. The electron beam is accelerated through a set of three drift tubes with the outer two held at a positive potential with respect to the inner, creating a trap of depth 220 V. The electron-beam energy is determined by the potential applied to the middle drift tube and determines the ion charge states present in the trap. A superconducting Helmholtz-pair magnet provides a 2.3-T axial magnetic flux density compressing the electron beam to a radius of $\sim$30 μm to give a high current density. Gadolinium ions were produced in a metal vapor vacuum arc (MEVVA) [28] ion source and injected into the EBIT where they were confined. The trap was emptied every 10 s to remove contaminating heavy ions that are present in the EBIT despite the ultrahigh-vacuum conditions (typically $\lesssim 10^{-7}$ Pa).

The spectra were recorded with a flat-field grazing-incidence spectrometer [29] in the wavelength range 3–17 nm. The spectrometer consists of a gold-coated-concave variable-spaced reflection grating with groove spacing of approximately 1200 lines mm^{-1}, and a liquid-nitrogen-cooled, back-illuminated CCD array having a matrix of 2048 × 512 pixels. The slit width was approximately 600 μm and the resolving power was approximately 350, which corresponds to a resolving limit of about 0.03 nm. The Zr filter was removed in order to improve the detector efficiency.

*deirdre.kilbane@ucd.ie

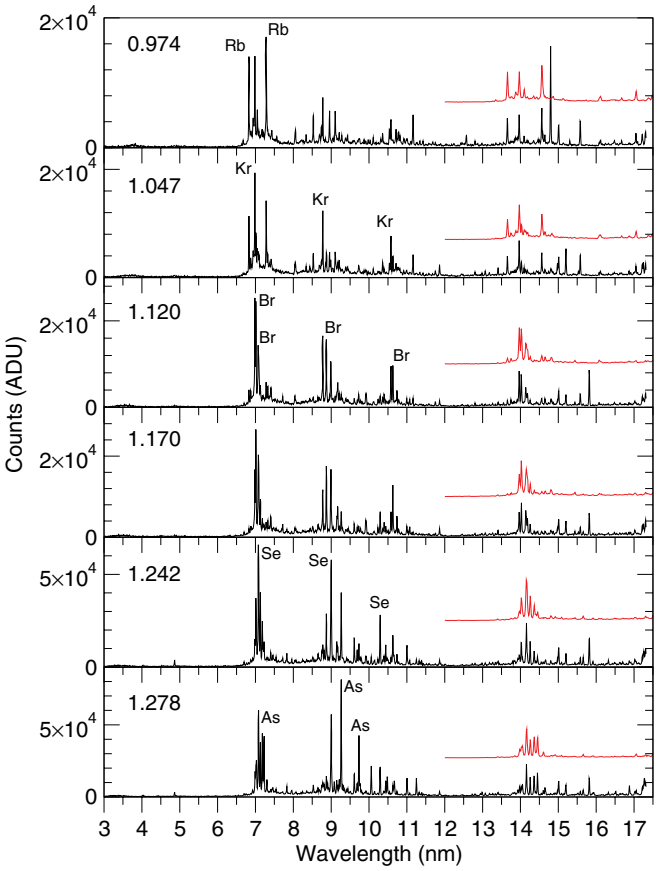

FIG. 1. (Color online) Experimental spectra of Gd ions. Nominal electron-beam energies (in kiloelectronvolts) are shown in the upper left corners. Second-order spectra are shifted vertically for clarity. Strong lines are indicated by their isoelectronic sequence.

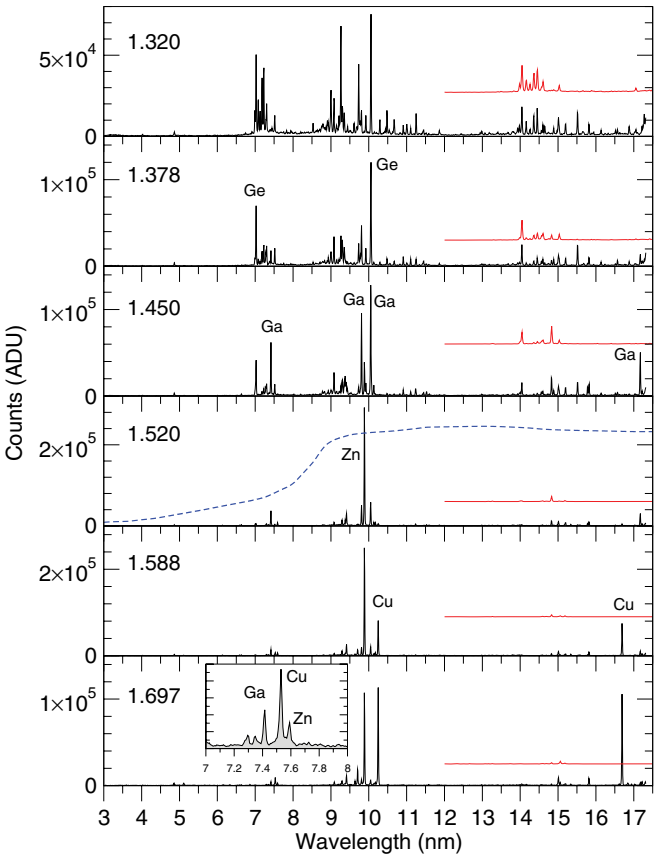

FIG. 2. (Color online) Experimental spectra of Gd ions. Nominal electron-beam energies (in kiloelectronvolts) are shown in the upper left corners. Second-order spectra are shifted vertically for clarity. Strong lines are indicated by their isoelectronic sequence. Dashed curve shows the spectrometer efficiency curve (in arbitrary units).

Nominal electron-beam energies were corrected for electron space-charge effects using the formula from [30]. The corrected energies ranging from about 0.95 to 1.63 keV, with beam currents of 10.5 and 37.5 mA, respectively, produced Rb-like $(27+)$ to Cu-like $(35+)$ ions of gadolinium. The spectra are shown in Figs. 1 and 2 along with the second-order spectra which are offset vertically for clarity. The spectra counts are the CCD analog-to-digital units (ADU) which result from binning each column to improve the signal-to-noise ratio. Each spectrum consisted of ten exposures of 60-s duration. A bias offset of 7400 counts/column was subtracted from all spectra and spurious signals from cosmic rays were removed. Calibration of the spectra was achieved by fitting a statistically weighted Gaussian profile to well-known reference lines of Xe, Ba, C, and O which have been compiled in [31]. The statistical errors in line positions were less than 0.001 nm. The final wavelength for each reference line is a weighted average of the wavelengths measured at various beam energies. The calibration curve was fitted with a weighted polynomial of the fourth order. The quadrature sum of the calibration uncertainty and the statistical uncertainty in fitting the gadolinium line centers results in a final uncertainty of $\sim$0.003 nm.

III. COLLISIONAL-RADIATIVE MODELING OF EBIT SPECTRA

The analysis of the observed gadolinium spectra was performed by CR modeling of the EBIT plasma assuming steady-state equilibrium and an electron density of $N_e = 10^{11}$ cm^{-3}. Identification of spectral lines was achieved by comparing calculated line positions and intensities with spectra measured at several electron-beam energies. A detailed CR modeling of ionization balance, level populations, and line intensities was successfully applied in our previous works on highly charged high-Z ions [24,32–35]. Here simulations were performed with the non-Maxwellian CR code NOMAD [26], utilizing atomic radiative and collisional data calculated with the Flexible Atomic Code (FAC) [36]. For a steady-state equilibrium analysis, full CR modeling of the EBIT plasma involving several dozens of ion stages and tens of thousands of energy levels is not necessary. Instead, the scale of CR modeling can be reduced without loss of accuracy because the population of ions is low for ions with ionization energies above the beam energy and for ions with charge much lower than the most abundant ion. Hence these ion stages have negligible contribution to the spectrum, and six to eight ion stages are enough to include in a typical simulation.

TABLE I. The ionization energies of the highly charged ions of Gd calculated with the flexible atomic code [36].

Ion	Sequence	Ground configuration	Ionization energy (eV)
Gd^{27+}	Rb	$4p^6 4d$	936
Gd^{28+}	Kr	$4s^2 4p^6$	1100
Gd^{29+}	Br	$4s^2 4p^5$	1142
Gd^{30+}	Se	$4s^2 4p^4$	1189
Gd^{31+}	As	$4s^2 4p^3$	1233
Gd^{32+}	Ge	$4s^2 4p^2$	1320
Gd^{33+}	Ga	$4s^2 4p$	1369
Gd^{34+}	Zn	$3d^{10} 4s^2$	1481
Gd^{35+}	Cu	$3d^{10} 4s$	1531

Accordingly, this was the extent of a "sliding window" for ions that was used in the calculations.

The dominant plasma processes occurring in the EBIT are radiative decay, electron-impact excitation and ionization, radiative recombination, and charge exchange (CX) recombination with the background neutral atoms. The ionization energies for the gadolinium ions studied in this work were calculated using FAC and are presented in Table I. They agree with the energies computed in [37] to within 1 eV. As in [25,35], the calculation of atomic data for a specific ion was performed in two steps. First, energy levels, radiative transition rates, and collisional excitation, ionization, and recombination cross sections were calculated for all singly excited (up to $n = 6$, 7, or 8, depending on ion complexity) and some doubly excited configurations, including excitations from inner shells. Noting that all observed spectral lines are due to $n = 4$–$n = 4$ transitions, a second calculation of energy levels was performed which included all possible excitations within the $n = 4$ complex. The energy levels of the ground configuration were then updated in the CR simulation with these new values. This produced wavelengths in much better agreement with experimental results, while the calculated intensities remained practically unaffected. The effect of CX with neutral atoms in the trap was also included in the simulations. The calculated spectral lines were convolved with the spectrometer efficiency curve shown by the dashed line in Fig. 2.

The simulated Rb-like to Cu-like spectra are presented in Fig. 3. One can notice two groups of lines: one near 7 nm, the position of which is almost independent of the ion charge, and another moving from about 8.7 nm for Kr-like ion to above 10 nm for the Cu-like ion. The shorter-wavelength lines are primarily due to $4p_{1/2}$-$4d_{3/2}$ electron jumps, for instance, the $4p^6\ {}^1S_0$–$4p^5\,4d\ (1/2,3/2)_1$ line at ≈6.9 nm in the Kr-like ion. The Zn- and Cu-like ions without $4p$ electrons in the ground state do not have strong $4p$-$4d$ transitions in the low-density plasma of EBITs. The longer-wavelength lines

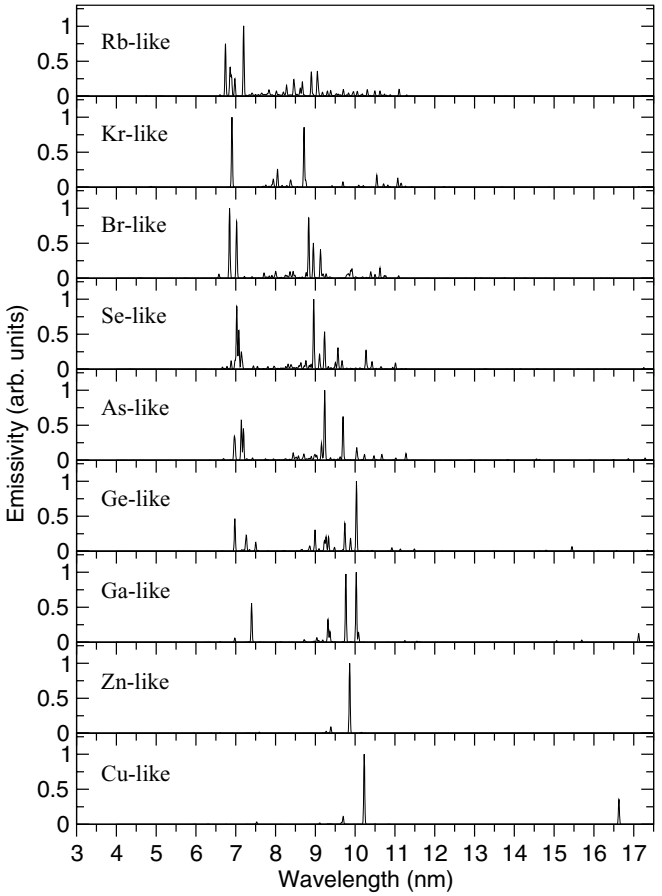

FIG. 3. Simulated spectra based on the CR code NOMAD for the $n = 4$–$n = 4$ transitions in gadolinium ions. Each charge state is indicated by its isoelectronic sequence.

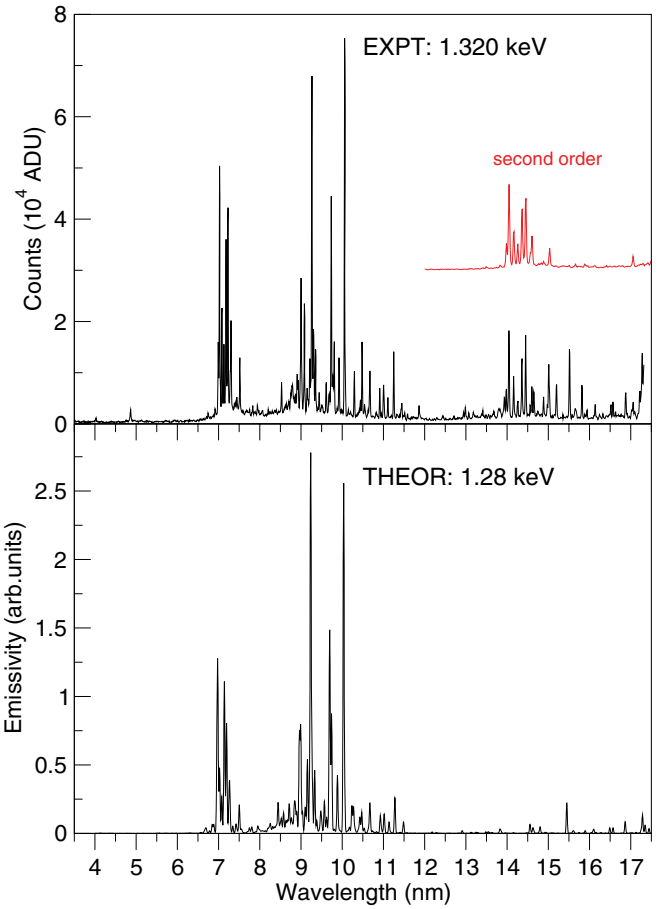

FIG. 4. (Color online) Comparison of the measured spectrum at 1.320 keV and calculated spectrum at 1.28 keV.

TABLE II. Wavelengths of spectral lines of highly charged ions of gadolinium. The uncertainties of other experimental results are given in units of the last significant digit. References: a– [8], b– [19], c– [6], d– [7], e– [20], f– [11], g– [14], h– [13], i– [17], j– [12], k– [41], l– [42], m– [43], n– [9], o– [15].

	Lower level		Upper level		λ_{expt} (nm)		λ_{theor} (nm)	
Ion	Conf.	State	Conf.	State	Current	Previous	Current	Previous
Gd^{31+} [As]	$4s^24p^3$ [2]	$(4p_-,4p_+^2)_{3/2}$	$4s4p^4$ [6]	$(4s_+,4p_+^2)_{5/2}$	17.279		17.2859	
Gd^{33+} [Ga]	$4s^24p$ [1]	$(4p_-)_{1/2}$	$4s4p^2$ [3]	$(4s_+)_{1/2}$	17.172		17.1246	
Gd^{31+} [As]	$4s^24p^3$ [3]	$(4p_-,4p_+^2)_{5/2}$	$4p^24d$ [7]	$(4d_-)_{3/2}$	16.879		16.8651	
Gd^{35+} [Cu]	$4s$ [1]	$(4s_+)_{1/2}$	$4p$ [2]	$(4p_-)_{1/2}$	16.692	16.688(3)[a]	16.6283	16.6369[a],16.6927[b]
Gd^{32+} [Ge]	$4p4d$ [10]	$(4p_-,4d_-)_2$	$4s4p^24d$ [28]	$(4s_+,4d_-)_2$	16.570		16.5712	
Gd^{31+} [As]	$4s^24p^3$ [4]	$(4p_-,4p_+^2)_{1/2}$	$4s4p^4$ [8]	$(4s_+,4p_+^2)_{1/2}$	16.518		16.4912	
Gd^{32+} [Ge]	$4s4p^3$ [9]	$((4s_+,4p_-)_1,4p_+^2)_3$	$4s4p^24d$ [28]	$(4s_+,4d_-)_2$	16.137		16.1050	
Gd^{33+} [Ga]	$4s^24p$ [2]	$(4p_+)_{3/2}$	$4s4p^2$ [6]	$((4s_+,4p_-)_1,4p_+)_{3/2}$	15.781		15.6953	
Gd^{32+} [Ge]	$4s^24p^2$ [3]	$(4p_-,4p_+)_2$	$4s4p^3$ [7]	$(4s_+,4p_+)_1$	15.516		15.4483	
Gd^{33+} [Ga]	$4s^24p$ [2]	$(4p_+)_{3/2}$	$4s4p^2$ [7]	$((4s_+,4p_-)_1,4p_+)_{1/2}$	15.198		15.0644	
Gd^{32+} [Ge]	$4s^24p^2$ [2]	$(4p_-,4p_+)_1$	$4s4p^3$ [7]	$(4s_+,4p_+)_1$	14.885		14.8017	
Gd^{33+} [Ga]	$4s^24p$ [1]	$(4p_-)_{1/2}$	$4s4p^2$ [4]	$((4s_+,4p_-)_0,4p_+)_{3/2}$	11.525		11.5533	
Gd^{32+} [Ge]	$4s^24p^2$ [2]	$(4p_-,4p_+)_1$	$4s4p^3$ [8]	$((4s_+,4p_-)_0,4p_+^2)_2$	11.446		11.4893	
Gd^{31+} [As]	$4s^24p^3$ [1]	$(4p_+)_{3/2}$	$4s4p^4$ [6]	$(4s_+,4p_+^2)_{5/2}$	11.250		11.2781	
Gd^{32+} [Ge]	$4s^24p^2$ [3]	$(4p_-,4p_+)_2$	$4s4p^3$ [9]	$((4s_+,4p_-)_1,4p_+^2)_3$	11.106		11.1357	
Gd^{30+} [Se]	$4s^24p^4$ [1]	$(4p_+^2)_2$	$4s4p^5$ [6]	$(4s_+,4p_+^3)_2$	11.003		11.0133	
Gd^{34+} [Ge]	$4s^24p^2$ [3]	$(4p_-,4p_+)_2$	$4p4d$ [10]	$(4p_-,4d_-)_2$	10.910		10.9232	
Gd^{31+} [As]	$4s^24p^3$ [1]	$(4p_+)_{3/2}$	$4p^24d$ [7]	$(4d_-)_{3/2}$	10.670		10.6690	
Gd^{29+} [Br]	$4p^5$ [1]	$(4p_+^3)_{3/2}$	$4p^44d$ [5]	$(4p_+^2,4d_-)_{5/2}$	10.629		10.6245	
Gd^{28+} [Kr]	$4p^6$ [1]	$(4p_+^4)_0$	$4p^54d$ [3]	$(4p_+^3,4d_-)_1$	10.578		10.5442	
Gd^{31+} [As]	$4s^24p^3$ [3]	$(4p_-,4p_+^2)_{5/2}$	$4p^24d$ [16]	$((4p_-,4p_+)_2,4d_-)_{7/2}$	10.481		10.4734	
Gd^{30+} [Se]	$4s^24p^4$ [1]	$(4p_+^2)_2$	$4p^34d$ [8]	$(4p_+,4d_-)_2$	10.439		10.4244	
Gd^{30+} [Se]	$4s^24p^4$ [1]	$(4p_+^2)_2$	$4p^34d$ [10]	$(4p_+,4d_-)_3$	10.292		10.2744	
Gd^{35+} [Cu]	$4s$ [1]	$(4s_+)_{1/2}$	$4p$ [3]	$(4p_+)_{3/2}$	10.247	10.2497(15)[c], 10.2459(15)[d] 10.243(3)[a]	10.2282	10.2309[d], 10.2473[b] 10.2395[a]
Gd^{34+} [Zn]	$4s4p$ [3]	$(4s_+,4p_-)_1$	$4p^2$ [8]	$(4p_-,4p_+)_2$	10.171	10.1584(20)[e]	10.1663	10.1378[e]
Gd^{34+} [Zn]	$4s4p$ [4]	$(4s_+,4p_+)_2$	$4p^2$ [9]	$(4p_+^2)_2$	10.137	10.1399(20)[e]	10.1272	10.0943[e]
Gd^{33+} [Ga]	$4s^24p$ [2]	$(4p_+)_{3/2}$	$4s^24d$ [9]	$(4d_-)_{3/2}$	10.133		10.0849	
Gd^{32+} [Ge]	$4s^24p^2$ [1]	$(4p_-^2)_0$	$4s4p^3$ [7]	$(4s_+,4p_-)_1$	10.052		10.0332	
Gd^{33+} [Ga]	$4s^24p$ [1]	$(4p_-)_{1/2}$	$4s4p^2$ [6]	$((4s_+,4p_-)_1,4p_+)_{3/2}$	10.050	10.045(20)[f], 10.060[g]	10.0278	9.966[f]
Gd^{32+} [Ge]	$4s^24p^2$ [2]	$(4p_-,4p_+)_1$	$4s4p^3$ [12]	$((4s_+,4p_-)_1,4p_+^2)_1$	9.921		9.8836	
Gd^{34+} [Zn]	$4s^2$ [1]	$(4s_+^2)_0$	$4s4p$ [5]	$(4s_+,4p_+)_1$	9.884	9.8824(20)[e], 9.8831(10)[h], 9.887(2)[j]	9.8628	9.8442[i], 9.8186[e], 9.8621[k], 9.8843[l], 9.8832[m]
Gd^{33+} [Ga]	$4s^24p$ [1]	$(4p_-)_{1/2}$	$4s4p^2$ [7]	$((4s_+,4p_-)_1,4p_+)_{1/2}$	9.807	9.811(20)[f]	9.7664	9.655[f]
Gd^{34+} [As]	$4s^24p^3$ [1]	$(4p_+)_{3/2}$	$4s4p^4$ [9]	$(4s_+,4p_+^2)_{3/2}$	9.732		9.6954	
Gd^{28+} [Kr]	$4p^6$ [1]	$(4p_+^4)_0$	$4p^54d$ [7]	$(4p_+^3,4d_+)_2$	9.726		9.6932	
Gd^{35+} [Cu]	$4p$ [3]	$(4p_+)_{3/2}$	$4d$ [5]	$(4d_+)_{5/2}$	9.704	9.7026(15)[d], 9.7074(15)[c]	9.6999	9.6962[d], 9.6958[n]
Gd^{30+} [Se]	$4s^24p^4$ [1]	$(4p_+^2)_2$	$4p^34d$ [11]	$(4p_+,4d_+)_4$	9.684		9.6719	
Gd^{35+} [Cu]	$4d$ [5]	$(4d_+)_{5/2}$	$4f$ [7]	$(4f_+)_{7/2}$	9.636	9.6349(15)[d], 9.6398(15)[c]	9.6598	9.6419[n], 9.6426[d]
Gd^{30+} [Se]	$4s^24p^4$ [1]	$(4p_+^2)_2$	$4s4p^5$ [12]	$(4s_+,4p_+^3)_1$	9.609		9.5688	
Gd^{34+} [Zn]	$4s4p$ [5]	$(4s_+,4p_+)_1$	$4s4d$ [14]	$(4s_+,4d_+)_2$	9.409	9.4085(20)[e]	9.3897	9.3651[e]
Gd^{33+} [Ga]	$4s^24p$ [2]	$(4p_+)_{3/2}$	$4s4p^2$ [11]	$(4s_+,4p_+^2)_{3/2}$	9.376		9.3183	
Gd^{32+} [Ge]	$4s4p^3$ [7]	$(4s_+,4p_+)_1$	$4s4p^24d$ [33]	$(4s_+,4d_+)_2$	9.352		9.3317	
Gd^{32+} [Ge]	$4s^24p^2$ [3]	$(4p_-,4p_+)_2$	$4p4d$ [15]	$(4p_-,4d_+)_3$	9.300		9.2711	
Gd^{31+} [As]	$4s^24p^3$ [1]	$(4p_+)_{3/2}$	$4p^24d$ [10]	$(4d_+)_{5/2}$	9.262		9.2345	
Gd^{29+} [Br]	$4p^5$ [1]	$(4p_+^3)_{3/2}$	$4p^44d$ [11]	$(4p_+^2,4d_+)_{1/2}$	9.172		9.1315	
Gd^{30+} [Se]	$4s^24p^4$ [2]	$(4p_+^2)_0$	$4p^34d$ [15]	$(4p_+,4d_+)_1$	9.146		9.1050	
Gd^{27+} [Rb]	$4p^64d$ [1]	$(4d_-)_{3/2}$	$4p^54d^2$ [23]	$((4p_+^3,4d_-)_2,4d_+)_{5/2}$	9.105		9.0503	
Gd^{35+} [Cu]	$4d$ [4]	$(4d_+)_{3/2}$	$4f$ [6]	$(4f_+)_{5/2}$	9.086	9.0875(15)[n], 9.0933(15)[c] 9.091(2)[o]	9.1108	9.0965[n], 9.0966[d]
Gd^{32+} [Ge]	$4s^24p^2$ [2]	$(4p_-,4p_+)_1$	$4p4d$ [16]	$(4p_-,4d_-)_1$	9.080		8.9921	
Gd^{30+} [Se]	$4s^24p^4$ [1]	$(4p_+^2)_2$	$4p^34d$ [14]	$(4p_+,4d_+)_3$	8.997		8.9595	
Gd^{29+} [Br]	$4p^5$ [1]	$(4p_+^3)_{3/2}$	$4p^44d$ [13]	$(4p_+^2,4d_+)_{3/2}$	8.991		8.9503	

TABLE II. *(Continued.)*

Ion	Lower level		Upper level		λ_{expt} (nm)		λ_{theor} (nm)	
	Conf.	State	Conf.	State	Current	Previous	Current	Previous
Gd^{27+} [Rb]	$4p^6 4d$ [1]	$(4d_-)_{3/2}$	$4p^5 4d^2$ [26]	$((4p_+^3,4d_-)_3,4d_+)_{3/2}$	8.955		8.8994	
Gd^{29+} [Br]	$4p^5$ [1]	$(4p_+^3)_{3/2}$	$4p^4 4d$ [14]	$(4p_+^2,4d_+)_{5/2}$	8.872		8.8336	
Gd^{28+} [Kr]	$4p^6$ [1]	$(4p_+^4)_0$	$4p^5 4d$ [9]	$(4p_+^3,4d_+)_1$	8.776		8.7156	
Gd^{27+} [Rb]	$4p^6 4d$ [1]	$(4d_-)_{3/2}$	$4p^5 4d^2$ [28]	$((4p_+^3,4d_-)_3,4d_+)_{1/2}$	8.525		8.4567	
Gd^{30+} [Se]	$4s^2 4p^4$ [1]	$(4p_+^2)_2$	$4p^3 4d$ [18]	$((4p_-,4p_+^2)_{3/2},4d_-)_2$	7.957		7.9583	
Gd^{30+} [Se]	$4s^2 4p^4$ [1]	$(4p_+^2)_2$	$4p^3 4d$ [20]	$((4p_-,4p_+^2)_{3/2},4d_-)_0$	7.826		7.8097	
Gd^{34+} [Zn]	$4s4p$ [3]	$(4s_+,4p_-)_1$	$4p^2$ [9]	$(4p_+^2)_2$	7.589	7.5954(20)[e]	7.5874	7.5836[e]
Gd^{30+} [Se]	$4s^2 4p^4$ [1]	$(4p_+^2)_2$	$4p^3 4d$ [23]	$((4p_-,4p_+^2)_{3/2},4d_+)_3$	7.540		7.5446	
Gd^{35+} [Cu]	$4p$ [2]	$(4p_-)_{1/2}$	$4d$ [4]	$(4d_-)_{3/2}$	7.527	7.5259(15)[d], 7.5316(15)[c], 7.524(2)[o]	7.5265	7.5274[n], 7.5277[d]
Gd^{32+} [Ge]	$4s^2 4p^2$ [1]	$(4p_-^2)_0$	$4s4p^3$ [12]	$((4s_+,4p_-)_1,4p_+^2)_1$	7.514		7.5026	
Gd^{30+} [Se]	$4s^2 4p^4$ [1]	$(4p_+^2)_2$	$4p^3 4d$ [25]	$((4p_-,4p_+^2)_{1/2},4d_-)_2$	7.458		7.4440	
Gd^{33+} [Ga]	$4s^2 4p$ [1]	$(4p_-)_{1/2}$	$4s^2 4d$ [9]	$(4d_-)_{3/2}$	7.413	7.414(20)[f]	7.3982	7.326[f]
Gd^{32+} [Ge]	$4s^2 4p^2$ [1]	$(4p_-^2)_0$	$4s4p^3$ [14]	$((4s_+,4p_-)_1,4p_+^2)_1$	7.300		7.2676	
Gd^{27+} [Rb]	$4p^6 4d$ [1]	$(4d_-)_{3/2}$	$4p^6 4f$ [39]	$(4f_-)_{5/2}$	7.282		7.1983	
Gd^{31+} [As]	$4s^2 4p^3$ [1]	$(4p_+)_{3/2}$	$4p^2 4d$ [21]	$((4p_-,4p_+)_1,4d_+)_{5/2}$	7.224		7.1941	
Gd^{31+} [As]	$4s^2 4p^3$ [1]	$(4p_+)_{3/2}$	$4p^2 4d$ [22]	$((4p_-,4p_+)_2,4d_-)_{3/2}$	7.179		7.1405	
Gd^{30+} [Se]	$4s^2 4p^4$ [1]	$(4p_+^2)_2$	$4p^3 4d$ [29]	$((4p_-,4p_+^2)_{5/2},4d_-)_2$	7.127		7.0771	
Gd^{30+} [Se]	$4s^2 4p^4$ [1]	$(4p_+^2)_2$	$4p^3 4d$ [30]	$((4p_-,4p_+^2)_{3/2},4d_-)_3$	7.079		7.0254	
Gd^{32+} [Ge]	$4s^2 4p^2$ [1]	$(4p_-^2)_0$	$4s^2 4p4d$ [16]	$(4p_-,4d_-)_1$	7.021		6.9775	
Gd^{29+} [Br]	$4p^5$ [1]	$(4p_+^3)_{3/2}$	$4p^4 4d$ [27]	$((4p_-,4p_+^2)_2,4d_-)_{5/2}$	7.010		6.8451	
Gd^{28+} [Kr]	$4p^6$ [1]	$(4p_+^4)_0$	$4p^5 4d$ [13]	$(4p_-,4d_-)_1$	6.982		6.9047	
Gd^{27+} [Rb]	$4p^6 4d$ [1]	$(4d_-)_{3/2}$	$4p^5 4d^2$ [45]	$(4p_-,4d_-^2)_{3/2}$	6.827		6.7410	
Gd^{34+} [Zn]	$4s4p$ [3]	$(4s_+,4p_-)_1$	$4s4d$ [14]	$(4s_+,4d_+)_2$	6.630		6.6085	

are due to several types of transitions: primarily, $4p_{3/2}$-$4d_{5/2}$ for lower ions and then $4s_{1/2}$-$4p_{3/2}$ in higher ions (Ga-, Zn-, and Cu-like) where the ground configuration has no $4p_{3/2}$ electrons. The presence of two groups of lines is well confirmed by the measured spectra shown in Figs. 1 and 2.

Comparison of experimental and calculated spectra is exemplified in Fig. 4, where the measurements at 1.32 keV are shown along with calculations at 1.28 keV. The lower energy used in the calculations reflects the effect of space charge on the beam electrons. It is obvious that a mere match of calculated and measured wavelengths is not sufficient for unambiguous identifications because of line overlaps, and therefore line intensity comparisons become crucially important. The accuracy of CR modeling is clear from this figure: the relative intensities of strong lines are reproduced so well that some lines can be identified even without any analysis of the beam-energy dependence of line intensities. Nonetheless, we did perform such analyses for all identified lines in the measured spectra.

IV. LINE IDENTIFICATIONS

The line identifications are given in Table II in the jj-coupling scheme as calculated with the FAC code. The numbers in brackets following the configurations are the calculated energy level number within the ion, where the ground state is level 1 and the first excited state is level 2, and so on. In addition to our experimental and calculated wavelengths, Table II shows wavelengths from other experiments and theoretical calculations. There is good agreement between the present and previously measured wavelengths to within the combined uncertainties, with two exceptions. The 10.171 nm and 7.589 nm lines in Zn-like Gd^{34+} were reported in Ref. [20] as having wavelengths of 10.1584 ± 0.002 nm and 7.5954 ± 0.002 nm, respectively. Nonetheless, the other three measured lines in Gd^{34+} agree between the present EBIT measurements and the laser-produced-plasma experiment of [20] to within 0.025%.

The $4s4p$-$4p^2$ 7.589 nm line was a subject of another recent study from magnetic fusion. Suzuki *et al.* [15] report two uncertain lines at 7.409 ± 0.002 nm (referred to as "c" in [15]) and 7.583 ± 0.002 nm ("e"), which were recorded in the Gd-pellet measurements on stellarator LHD at an electron temperature of about 2 keV. The relative intensities of these lines and of the third line at 7.524 nm (Cu-like ion) in LHD agree well with our EBIT measurements for the beam energy of 1.697 keV, as can be seen from the inset in Figs. 2 and 4 in Ref. [15]. This agreement provides evidence that our 7.589 nm line and the 7.583 nm line from LHD measurements are the same. Also, the authors of Ref. [15] tentatively assigned the 7.409 nm line to the Zn-like ion, although Fournier *et al.* [11] claimed this line to belong to the Ga-like ion. Our CR modeling confirms the original identification of Ref. [11] for the 7.409 nm line, although our measured wavelength of 7.413 nm for this resonance transition $4s^2 4p$-$4s^2 4d$ is slightly longer than the LHD value.

The good resolution of the measured spectra allows us to confirm identification of some newly identified lines using the Ritz combination principle. Consider, for instance, the following lines in the Ge-like ion: 16.570 nm, 16.137 nm, 11.106 nm, and 10.910 nm. These lines connect levels 9 and 10 with level 28 and level 3 (see Table II). Therefore, the energy difference between levels 9 and 10 calculated from the differences of wavenumbers for two pairs of transitions should be the same. Indeed, the 9–28 and 10–28 lines give $\Delta E_{\mathrm{Ge}}(9-10) \approx 16\,194\ \mathrm{cm}^{-1}$, and the 3–9 and 3–10 transitions result in a close value of $\approx 16\,176\ \mathrm{cm}^{-1}$. A similar Ritz analysis for the spectral lines connecting levels 1 and 2 with levels 6, 7, and 9 in the Ga-like ion also confirms our identifications. The average value of $\Delta E_{\mathrm{Ga}}(1-2) = 361\,590 \pm 220\ \mathrm{cm}^{-1}$ agrees very well with the the semiempirical value of $361\,529\ \mathrm{cm}^{-1}$ [38], and slightly worse with the relativistic many-body theory value of $361\,913\ \mathrm{cm}^{-1}$ [39]; however, the multiconfiguration Dirac-Fock calculation of Ref. [40] gave a lower value of $360\,692\ \mathrm{cm}^{-1}$.

V. CONCLUSION

The EUV spectra from highly-charged ions of Gd were measured in the NIST EBIT. Ion stages of Rb-like to Cu-like gadolinium ions were produced by varying the beam energy from 0.95 keV to 1.7 keV. Collisional-radiative modeling of the EBIT plasma led to the identification of 59 new lines between 6.6 and 17.5 nm. These data are expected to be of use in future modeling of Gd plasmas in the development of next generation sources for EUV lithography.

ACKNOWLEDGMENTS

We thank Yuri Podpaly for independently confirming the calibration, wavelength determination, and error analysis. This work was supported by Science Foundation Ireland under Principal Investigator Research Grant 07/IN.1/I1771 and in part by the Office of Fusion Energy Sciences of the US Department of Energy.

[1] S. S. Churilov, R. R. Kildiyarova, A. N. Ryabtsev, and S. V. Sadovsky, Phys. Scr. **80**, 045303 (2009).
[2] T. Otsuka, D. Kilbane, T. Higashiguchi, N. Yugami, T. Yatagai, W. Jiang, A. Endo, P. Dunne, and G. O'Sullivan, Appl. Phys. Lett. **97**, 111503 (2010).
[3] T. Otsuka, D. Kilbane, T. Higashiguchi, N. Yugami, T. Yatagai, W. Jiang, A. Endo, P. Dunne, and G. O'Sullivan, Appl. Phys. Lett. **97**, 231503 (2010).
[4] D. Kilbane and G. O'Sullivan, J. Appl. Phys. **108**, 104905 (2010).
[5] A. Sasaki, K. Nishihara, A. Sunahara, H. Furukawa, T. Nishikawa, and F. Koike, Appl. Phys. Lett. **97**, 231501 (2010).
[6] J. Reader and G. Luther, Phys. Scr. **24**, 732 (1981).
[7] G. A. Doschek, U. Feldman, C. M. Brown, J. F. Seely, J. O. Ekberg, W. E. Behring, and M. C. Richardson, J. Opt. Soc. Am. B **5**, 243 (1988).
[8] J. F. Seely, U. Feldman, A. W. Wouters, J. L. Schwob, and S. Suckewer, Phys. Rev. A **40**, 5020 (1989).
[9] J. F. Seely, C. M. Brown, and U. Feldman, At. Data Nucl. Data Tables **43**, 145 (1989).
[10] M. Finkenthal, S. Lippmann, L. K. Huang, H. W. Moos, Y. T. Lee, N. Spector, A. Zigler, and E. Yarkoni, Phys. Scr. **41**, 445 (1990).
[11] K. B. Fournier, W. H. Goldstein, A. Osterheld, M. Finkenthal, S. Lippmann, L. K. Huang, H. W. Moos, and N. Spector, Phys. Rev. A **50**, 2248 (1994).
[12] J. Reader and G. Luther, Phys. Rev. Lett. **45**, 609 (1980).
[13] N. Acquista and J. Reader, J. Opt. Soc. Am. B **1**, 649 (1984).
[14] P. Mandelbaum, M. Finkenthal, E. Meroz, J. L. Schwob, J. Oreg, W. H. Goldstein, M. Klapisch, L. Osterheld, A. BarShalom, S. Lippman, L. K. Huang, and H. W. Moos, Phys. Rev. A **42**, 4412 (1990).
[15] C. Suzuki, F. Koike, I. Murakami, N. Tamura, and S. Sudo, J. Phys. B: At. Mol. Opt. Phys. **45**, 135002 (2012).
[16] I. P. Grant, B. J. McKenzie, P. H. Norrington, D. F. Mayers, and N. C. Pyper, Comput. Phys. Commun. **21**, 207 (1980).
[17] J. Sugar, V. Kaufman, D. H. Baik, Y.-K. Kim, and W. L. Rowan, J. Opt. Soc. Am. B **8**, 1795 (1991).
[18] J. P. Desclaux, Comput. Phys. Commun. **9**, 31 (1975).
[19] Y.-K. Kim, D. H. Baik, P. Indelicato, and J. P. Desclaux, Phys. Rev. A **44**, 148 (1991).
[20] C. M. Brown, J. F. Seely, D. R. Kania, B. A. Hammel, C. A. Back, R. W. Lee, A. Bar-Shalom, and W. E. Behring, At. Data Nucl. Data Tables **58**, 203 (1994).
[21] A. Bar-Shalom, M. Klapisch, and J. Oreg, J. Quant. Spectrosc. Radiat. Transfer **71**, 169 (2001).
[22] M. Klapisch, Comput. Phys. Commun. **2**, 269 (1971).
[23] M. Klapisch, J. L. Schwob, B. S. Fraenkel, and J. Oreg, J. Opt. Soc. Am. **67**, 148 (1977).
[24] Yu. Ralchenko, J. Reader, J. M. Pomeroy, J. N. Tan, and J. D. Gillaspy, J. Phys. B: At. Mol. Opt. Phys. **40**, 3861 (2007).
[25] I. Draganić, Yu. Ralchenko, J. Reader, J. D. Gillaspy, J. N. Tan, J. M. Pomeroy, S. M. Brewer, and D. Osin, J. Phys. B: At. Mol. Opt. Phys. **44**, 025001 (2011).
[26] Yu. V. Ralchenko and Y. Maron, J. Quant. Spectrosc. Radiat. Transfer **71**, 609 (2001).
[27] J. D. Gillaspy, Phys. Scr. T **71**, 99 (1997).
[28] G. E. Holland, C. N. Boyer, J. F. Seely, J. N. Tan, J. M. Pomeroy, and J. D. Gillaspy, Rev. Sci. Instrum. **76**, 073304 (2005).
[29] B. Blagojević, E.-O. L. Bigot, K. Fahy, A. Aguilar, K. Makonyi, E. Takács, J. N. Tan, J. M. Pomeroy, J. H. Burnett, J. D. Gillaspy, and J. R. Roberts, Rev. Sci. Instrum. **76**, 083102 (2005).
[30] J. D. Gillaspy, T. Lin, L. Tedesco, J. N. Tan, J. M. Pomeroy, J. M. Laming, N. Brickhouse, G.-X. Chen, and E. Silver, Astrophys. J. **728**, 132 (2011).
[31] D. Osin, J. Reader, J. D. Gillaspy, and Yu. Ralchenko (unpublished).
[32] Yu. Ralchenko, J. N. Tan, J. D. Gillaspy, J. M. Pomeroy, and E. Silver, Phys. Rev. A **74**, 042514 (2006).
[33] Yu. Ralchenko, I. N. Draganić, J. N. Tan, J. D. Gillaspy, J. M. Pomeroy, J. Reader, U. Feldman, and G. E. Holland, J. Phys. B **41**, 021003 (2008).

[34] J. D. Gillaspy, I. N. Draganić, Y. Ralchenko, J. Reader, J. N. Tan, J. M. Pomeroy, and S. M. Brewer, Phys. Rev. A **80**, 010501 (2009).
[35] Yu. Ralchenko, I. N. Draganić, D. Osin, J. D. Gillaspy, and J. Reader, Phys. Rev. A **83**, 032517 (2011).
[36] M. F. Gu, Can. J. Phys. **86**, 675 (2008).
[37] G. C. Rodrigues, P. Indelicato, J. P. Santos, P. Patte, and F. Parente, At. Data Nucl. Data Tables **86**, 117 (2004).
[38] L. J. Curtis, Phys. Rev. A **35**, 2089 (1987).
[39] U. I. Safronova, T. E. Cowan, and M. S. Safronova, Phys. Lett. A **348**, 293 (2006).
[40] M. A. Ali, Phys. Scr. **55**, 159 (1997).
[41] F. Hu, J.-M. Yang, C.-K. Wang, X.-F. Zhao, H.-P. Zang, G. Jiang, and L.-H. Hao, At. Data Nucl. Data Tables **98**, 301 (2012).
[42] U. I. Safronova and M. S. Safronova, J. Phys. B **43**, 074025 (2010).
[43] M. H. Chen and K. T. Cheng, J. Phys. B **43**, 074019 (2010).